International Journal of Microwave and Wireless Technologies

cambridge.org/mrf

Measurement of intrinsic nonlinear parameters for microwave ferromagnetic materials using coated transmission-line and LNS-FDTD methods

Xiaolong Zhao[1] and Xiaojian Xiang[2]

[1]School of Microelectronics, Faculty of Electronic and Information Engineering, Xi'an Jiaotong University, Xi'an, China and [2]Institute of Superlubricity Technology, Research Institute of Tsinghua University in Shenzhen, Shenzhen, China

Research Paper

Cite this article: Zhao X, Xiang X (2026) Measurement of intrinsic nonlinear parameters for microwave ferromagnetic materials using coated transmission-line and LNS-FDTD methods. *International Journal of Microwave and Wireless Technologies* **18**(4), 625–631. https://doi.org/10.1017/S1759078726103572

Received: 4 February 2026 UTC
Revised: 10 June 2026 UTC
Accepted: 15 June 2026 UTC
First published online: 24 July 2026 UTC

Keywords
Nonlinear effect; Passive intermodulation; Transmission line; Full wave simulation; Ferromagnetic material

Corresponding author: Xiaolong Zhao; Email: zhaoxiaolong@xjtu.edu.cn

Abstract

This work proposes two methods for evaluating the intrinsic nonlinear parameters for the microwave ferromagnetic materials, which play an important role in the development of low passive-intermodulation devices. We find that the product of the nonlinear permeability and the skin depth serves as the intrinsic nonlinear parameter governing the passive intermodulation (PIM) effect. Analytical and numerical models are proposed to extract it from the experiments. For the coated transmission line method, an analytical expression for the relationship between PIM and the nonlinear parameter is derived. For the linearity–nonlinearity-separation (LNS) Finite Difference Time Domain (FDTD) full-wave method, a PIM simulation algorithm suitable for thin coating layers is established. Both methods are validated using a nickel-plated microstrip line. The extraction results from the two approaches are in good agreement, confirming the consistency and feasibility of the proposed measurement methods.

Introduction

Ferromagnetic thin-film materials and coatings are widely used for electromagnetic shielding and in tunable devices [1–6]. However, their inherent nonlinearity can give rise to the passive intermodulation (PIM) and the radiated spurious emissions at new frequencies, making the study of their nonlinear effects highly significant.

Experimental results have shown that ferromagnetic material can cause the PIM effect in microwave components. Aldo De Sabata et al. [7] studied the problem of intermodulation distortions introduced by ferromagnetic material inclusions in the construction of equipment used for transmission and processing of Global System for Mobile Communications (GSM) signals. J. Henrie et al. [8] tested PIM of coaxial connections with different types, indicating that nickel material could increase the PIM value by more than 30 dB. Qiuyan Jin et al. [9, 10]. investigated the effects of coating thickness and material properties on PIM of coaxial connectors, and pointed out that the nickel underplate layer and the iron in the base brass were regarded as the primary nonlinear sources of PIM.

Given that the nonlinearity of ferromagnetic materials can lead to PIM and radiated spurious emissions, can we quantitatively evaluate this nonlinearity? Keyue Zhang et al. [11] designed a 2.6 GHz substrate integrated slot waveguide, which can be used to compare the PIM effect of different materials. However, the nonlinear parameters of the materials are still unknown.

To quantitatively extract the nonlinear parameters, we need to build a measurement platform that we can physically model. A transmission line is one of the appropriate choices, due to the mature transmission line theory. D. S. Kozlov et al. [12] put the pencil mark on the microstrip line and tested the PIM effect in order to investigate the mechanisms of PIM generation. In 2023, X. Zhao et al. proposed a linearity–nonlinearity-separation (LNS) FDTD method to numerically calculate the PIM effect induced by the material nonlinearity [13]. In 2024, X. Zhao et al. also derived closed-form equations for PIM calculation of transmission lines [14, 15]. Although these works have revealed the patterns and influencing factors of microstrip-line PIM, methods for extracting the nonlinear physical parameters of the materials themselves have not yet been thoroughly investigated.

In this work, we propose two extraction methods of intrinsic nonlinear parameters for microwave ferromagnetic materials, that is, the coated transmission-line method and the LNS-FDTD full-wave method. The ferromagnetic material is coated or plated on the surface of a

© The Author(s), 2026. Published by Cambridge University Press in association with The European Microwave Association.

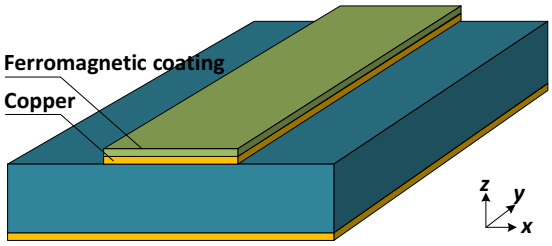


Figure 1. Schematic diagram of a ferromagnetic-material-coated microstrip line.

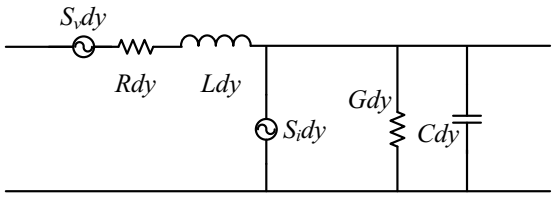


Figure 2. Schematic of the equivalent circuit for a microstrip line with nonlinearity.

microstrip line, and analytical equations between the intrinsic nonlinear parameter and the PIM value were deduced to extract this parameter. In addition, the LNS-FDTD simulation method was also introduced to compare with the coated transmission line model.

Coated transmission-line method

The fact that a microstrip line can be analytically modeled with transmission line theory makes it an ideal measurement platform. The microwave ferromagnetic thin film can be coated or plated onto the surface of the upper conductor of a microstrip line, as shown in Figure 1. A dual-carrier signal is fed into the microstrip line. Because the permeability of the ferromagnetic material depends on the magnetic field, i.e., its constitutive relation is nonlinear, the signals propagating along the microstrip line generate nonlinear signal components. Since the nonlinear signals carry the information of the materials' nonlinear parameters, we can extract them by establishing the relationship between these nonlinear signals and the nonlinear parameters. In the following, transmission line theory is employed to derive the relationship between the PIM of a ferromagnetic-material-coated microstrip line and its third-order permeability.

According to Ref. [15], the equivalent circuit of a *dy* length microstrip line with nonlinearity can be illustrated as Figure 2, where *R, L, G*, and *C* are the resistance, inductance, conductance, and capacitance per unit length of the microstrip line, and S_v and S_i are the controlled voltage and current sources per unit length, respectively. S_v can model the nonlinearity from *R* and *L*, while the nonlinearity of *G* and *C* can be modeled using S_i.

For a microstrip line with ferromagnetic coating, its nonlinearity is caused by the inductance nonlinearity. The nonlinear inductance can be expressed using a polynomial function:

$$\tilde{L} = L + L_2 i^2 + L_4 i^4 + \cdots, \tag{1}$$

where L is the linear part inductance, L_2 and L_4 are the nonlinear coefficients, and i is the current.

Therefore, the voltage across the nonlinear conductance can be denoted as:

$$dv = \frac{d\left(\tilde{L}dy \cdot i\right)}{dt} = (Ldy)\cdot\frac{di}{dt} + (L_2 dy)\cdot\frac{di^3}{dt} + (L_4 dy)\cdot\frac{di^5}{dt} + \cdots. \tag{2}$$

In this work, we mainly consider the third-order PIM model; therefore, we can consider only the third-order nonlinear term, that is

$$dv = \frac{d\left(\tilde{L}dy \cdot i\right)}{dt} \approx (Ldy)\cdot\frac{di}{dt} + (L_2 dy)\cdot\frac{di^3}{dt}. \tag{3}$$

For the PIM test, a two-tone excitation is generally used, i.e.,

$$i_0 = I_1\cos(2\pi f_1 t + \phi_1) + I_2\cos(2\pi f_2 t + \phi_2), \tag{4}$$

where I_1 and I_2 are the magnitudes of the two-tone signals, f_1 and f_2 are the frequencies, ϕ_1 and ϕ_2 are the initial phases, and t is the time.

Applying the harmonic balance method to Eq. (2) and considering the presence of the i^3 term, it can be concluded that the expression must contain the third-order intermodulation frequency components at $2f_1 - f_2$ and $2f_2 - f_1$. Extracting the $2f_1 - f_2$ component and combining it with Eq. (4), the expression for the $2f_1 - f_2$ component is obtained as:

$$dV_{fPIM} \approx (Ldy)\cdot(j2\pi f_{PIM})\, I_{fPIM} + (L_2 dy)\cdot\frac{3}{4}I_1^2 I_2\,(j2\pi f_{PIM}), \tag{5}$$

where V_{fPIM} and I_{fPIM} are the voltage and current signals at the PIM frequency, $f_{PIM} = 2f_1 - f_2$. The second term on the right-hand side of the expression can be regarded as a source term, from which the PIM signal is excited. Hence, we write:

$$S_v dy \approx (L_2 dy)\cdot\frac{3}{4}I_1^2 I_2\,(j2\pi f_{PIM}). \tag{6}$$

It should be noted that Eq. (6) only accounts for amplitude information. Since the signal phase varies along the microstrip line, the expression for the controlled voltage source that incorporates the phase information becomes:

$$S_v dy \approx (L_2 dy)\cdot\frac{3}{4}I_{10}^2 I_{20}\,(j2\pi f_{PIM})\exp\left(-j\left(2k_1 - k_2\right)y\right), \tag{7}$$

where I_{10} and I_{20} are the amplitudes of current at the input port, and k_1 and k_2 are the propagation constants.

The voltage drop generated by $S_v dy$ at the input port is $S_v \cdot \exp(-jky)dy$, where $k = 2k_1 - k_2$. By integrating this voltage drop over the input port, the reverse PIM voltage wave can be obtained.

$$\begin{aligned} V_{r,PIM} &= \int_0^L S_v \exp(-jky)\, dy \\ &= -\frac{3\pi}{4k}L_2 I_1^2 I_2\,(f_{PIM})\left[\exp(-j2kL) - 1\right] \end{aligned} \tag{8}$$

Therefore:

$$\left|V_{r,PIM}\right| = \frac{3\pi}{2k}L_2 I_1^2 I_2\,(f_{PIM})\left|\sin(kL)\right|. \tag{9}$$

Similarly, the transmitted PIM voltage wave at the output port is obtained as:

$$\begin{aligned} V_{f,PIM} &= \int_0^L S_v \exp(-jk(L-y))\, dy \\ &= \frac{3}{4}L_2 I_1^2 I_2\,(j2\pi f_{PIM})\, L\exp(-jkL). \end{aligned} \tag{10}$$

https://doi.org/10.1017/S1759078726103572 Published online by Cambridge University Press

Then:

$$\left|V_{f,PIM}\right| = \frac{3\pi}{2} L_2 I_1^2 I_2 \left(f_{PIM}\right) L. \tag{11}$$

Thus, the relationship between the PIM voltage and the nonlinear coefficient L_2 has been established.

Next, if the relationship between L_2 and the intrinsic nonlinear parameters of the ferromagnetic material is obtained, the connection between PIM and the intrinsic parameters can be established.

The internal inductance per unit length of the ferromagnetic coating can be expressed as:

$$L_{\text{int},Ni} = \frac{\mu\delta}{W}, \tag{12}$$

where μ is the permeability, δ the skin depth, and W the width of the microstrip line. For a ferromagnetic material, its permeability is the function of magnetic field strength.

That is:

$$\mu\left(H\right) = \mu_0\mu_r + \mu_0\mu_r^{(3)}|H|^2 + \cdots, \tag{13}$$

where μ_0 and μ_r are the vacuum and relative permeabilities, respectively, and $\mu_r^{(3)}$ is the third-order permeability.

Since I is the total current propagating along the upper conductor and the ferromagnetic coating exists only on its top surface, only a fraction of the current flows through the coating layer. Let this fraction be denoted by k_0. Then the magnetic field H due to that portion of the current can be estimated as $k_0 I/W$. Additionally, we must consider only the fraction ξ of this magnetic field that couples back into the microstrip line to form a quasi-TEM wave. Given the approximate symmetry between these two processes, we assume the coupling efficiency satisfies $\xi \approx k_0$. Therefore,

$$\mu\left(H\right) \approx \mu_0\mu_r + \mu_0\mu_r^{(3)}k_0^3\left(\frac{I}{W}\right)^2 + \cdots. \tag{14}$$

By substituting Eq. (14) into Eq. (12), we have:

$$L_{\text{int},Ni} \approx \mu_0\mu_r\frac{\delta}{W} + \mu_0\mu_r^{(3)}k_0^3\frac{\delta}{W^3}I^2 + \cdots. \tag{15}$$

Comparing Eq. (15) and Eq. (1), we obtain:

$$L_2 = \frac{\mu_0 k_0^3}{W^3}\delta\mu_r^{(3)}. \tag{16}$$

Thus, we find the relationship between the equivalent nonlinear parameter L_2 and the material parameters. In Eq. (16), both $\mu_r^{(3)}$ and δ are related to the material parameters determining its nonlinear performance; therefore, we treat the product of these two parameters as its intrinsic nonlinear parameter.

According to the microwave theory, the intrinsic impedance of a good conductor is

$$\eta = (1+j)\sqrt{\frac{\omega\mu}{2\sigma}} = \frac{1}{\sigma\delta} + j\omega\left(\frac{1}{2}\mu\delta\right), \tag{17}$$

where σ is the conductivity. $1/(\sigma\delta)$ represents the surface resistance, while $1/(2\mu\delta)$ is regarded as the surface inductance. For magnetic materials, μ is a function of the magnetic field strength, i.e., $\mu(H)$. This leads to nonlinearity. Consequently, this nonlinearity is viewed as originating from the nonlinear behavior of the surface inductance.

Therefore, the surface inductance can be expressed as:

$$\begin{aligned}\frac{1}{2}\mu\delta = \sqrt{\frac{\mu}{2\omega\sigma}} &= \left\langle\frac{1}{2}\mu\delta\right\rangle\sqrt{1+\frac{\mu_r^{(3)}|H|^2+\cdots}{\mu_r}} \\ &= \left\langle\frac{1}{2}\mu\delta\right\rangle\left(1+\frac{1}{2}\frac{\mu_r^{(3)}|H|^2}{\mu_r}+\cdots\right), \\ &= \left\langle\frac{1}{2}\mu\delta\right\rangle + \frac{1}{4}\mu_0\mu_r^{(3)}\left\langle\delta\right\rangle|H|^2+\cdots\end{aligned} \tag{18}$$

where $<1/(2\mu\delta)>$ represents the surface inductance under the condition of neglecting nonlinear effects. Eq. (18) shows that the third-order PIM is primarily influenced by $\frac{1}{4}\mu_0\mu_r^{(3)}\delta|H|^2$. Since the nonlinear term is much smaller than the linear term at microwave frequencies, $<\delta> \approx \delta$. Therefore, we define the material-dependent parameter $\delta\mu_r^{(3)}$ as the intrinsic nonlinear parameter.

Using Eqs. (9), (11), and (16), the relationship between PIM power and the intrinsic nonlinear parameter is derived.

$$P_{IM3,\text{forward}} = \frac{\left|V_{f,PIM}\right|^2}{2Z_0} = \frac{9\pi^2}{8Z_0}\left(I_1^2 I_2 L f_{PIM}\frac{\mu_0 k_0^3}{W^3}\right)^2\left(\delta\mu_r^{(3)}\right)^2, \tag{19a}$$

$$\begin{aligned}P_{IM3,\text{reverse}} &= \frac{\left|V_{r,PIM}\right|^2}{2Z_0} \\ &= \frac{9\pi^2}{8k^2Z_0}\left(I_1^2 I_2 f_{PIM}\frac{\mu_0 k_0^3}{W^3}\left|\sin\left(kL\right)\right|\right)^2\left(\delta\mu_r^{(3)}\right)^2,\end{aligned} \tag{19b}$$

where Z_0 is the characteristic impedance, which is 50 Ω.

LNS-FDTD full-wave method

Since the nonlinear effects of ferromagnetic materials can be described by a nonlinear constitutive equation, their resulting nonlinear responses, such as PIM and harmonics, can be simulated in a full-wave solver by incorporating such a nonlinear constitutive relation. Then, the nonlinear parameters can be extracted by adjusting the nonlinear parameters until the simulated results match the experimental data. Because the nonlinear effect, for example, PIM, is usually weak, the simulation process can adopt the "linearity-nonlinearity separation" method [13, 16]. It should be noted that the thickness of the ferromagnetic coating is typically on the micron scale, which is much smaller than the usual mesh size. Therefore, a special modeling method is required in the full-wave simulation. In the following, a PIM simulation method for ferromagnetic-material-coated microstrip lines is developed, thereby enabling the extraction of third-order nonlinear parameters via full-wave simulation.

Let's start with the nonlinear constitutive equation for an isotropic ferromagnetic material with third-order magnetic nonlinearity.

$$B = \mu_0\mu_r H + \mu_0\mu_r^{(3)}|H|^2 H, \tag{20}$$

where B is the magnetic flux density.

Neglecting the nonlinear term in Eq. (20), its zeroth-order approximation is given by:

$$B_0 = \mu_0\mu_r H_0. \tag{21}$$

By subtracting Eq. (21) from Eq. (20), we have:

$$B_p = \mu_0\mu_r H_p + \mu_0\mu_r^{(3)}|H|^2 H, \tag{22}$$

https://doi.org/10.1017/S1759078726103572 Published online by Cambridge University Press

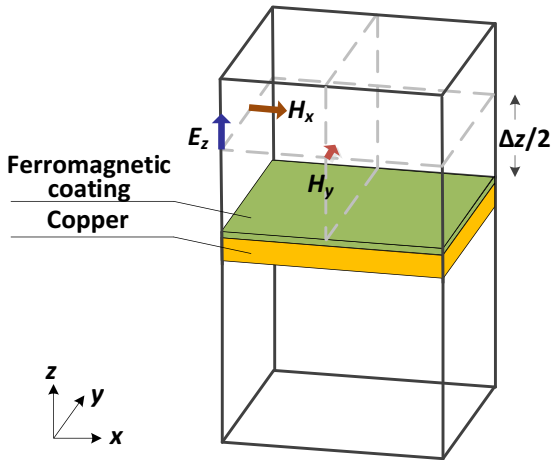


Figure 3. The definition positions of the tangential magnetic fields do not coincide with the conductor surface in the Yee grid.

where $B = B_0 + B_p$, and $H = H_0 + H_p$.

Because the nonlinearity is usually weak for microwave applications, we simplify Eq. (3) to be

$$B_p = \mu_0 \mu_r H_p + M, \tag{23}$$

where $M = \mu_0 \mu_r^{(3)} |H_0|^2 H_0$.

Let the surface tangential magnetic field be $H_0(t)$. Under the good-conductor approximation, the field inside the conductor decays approximately exponentially:

$$H_0(z,t) \approx H_0(t) \exp(-z/\delta). \tag{24}$$

The equivalent surface magnetization is defined as the depth integral of the volume magnetization:

$$\begin{aligned} M_s(t) &= \int_0^\infty M(z,t)\, dz \\ &= \int_0^\infty \mu_0 \mu_r^{(3)} |H_0|^2 H_0 dz \\ &= \frac{1}{3} \mu_0 \left(\delta \mu_r^{(3)}\right) |H_0(t)|^2 H_0(t). \end{aligned} \tag{25}$$

To incorporate this source term into the FDTD update equations, it must be converted into a volume magnetic current density acting on the magnetic-field grid. Physically, this corresponds to "spreading" the surface-concentrated magnetic current over the nearest half-grid thickness ($\Delta z/2$), because the tangential magnetic field is defined only on the surface center of the Yee mesh grid as shown in Figure 3.

Therefore,

$$M_v(t) = \frac{2}{\Delta z} M_s(t) \approx \frac{2}{3\Delta z} \mu_0 \left(\delta \mu_r^{(3)}\right) |H_0(t)|^2 H_0(t)\, \delta_{k,k_{suf}}. \tag{26}$$

where $\delta_{k,\,ksurf}$ is the Kronecker delta, which ensures that the source term exists only at the surface layer.

According to Maxwell's equations, we have:

$$\begin{aligned} \nabla \times E_p &= -\frac{\partial B_p}{\partial t} = -\frac{\partial \left(\mu_0 \mu_r H_p + M\right)}{\partial t} \\ &= -\mu_0 \mu_r \frac{\partial H_p}{\partial t} - \frac{2}{3\Delta z} \mu_0 \left(\delta \mu_r^{(3)}\right) \\ &\quad \times \frac{\partial |H_0(t)|^2 H_0(t)}{\partial t} \delta_{k,k_{suf}}. \end{aligned} \tag{27}$$

Thus, the equation for the nonlinear part field is obtained, and we use it in the FDTD solver to simulate PIM of the ferromagnetic-material-coated microstrip line. The implementation of the simulation can refer to [13, 16]. Eq. (27) shows that only the intrinsic nonlinear parameter $\delta \mu_r^{(3)}$ is unknown. Therefore, if we compare the experimental data with the simulation results, we can extract this parameter.

Intrinsic nonlinear parameter extraction of Ni coating

PIM experiments

This section validates the nonlinear parameter extraction method by plating a nickel layer on a microstrip line and measuring its PIM effects. The microstrip line is fabricated using a copper-clad laminate with a dielectric constant of 3.5 and a thickness of 1 mm, and a 0.5-oz nickel layer is electroplated onto its upper conductor, as shown in Figure 4(a). The PIM measurement equipment (BXT Technologies) is shown in Figure 4(b). The schematic block diagram of the measurement setup is given in Figure 5. Two carrier signals are set at 728 and 746 MHz, respectively. After amplification, they are combined and fed through Duplexer 1 into the microstrip line under test. The transmitted carriers continue through Duplexer 2 and are absorbed by a low-PIM load. The intermodulation products generated by the nickel-plated microstrip line propagate toward both its input and output ports. The PIM signal traveling toward the input port passes through Duplexer 1 and is sampled by a spectrum analyzer, which is referred to as the reflected PIM. The PIM signal traveling toward the output port passes through Duplexer 2 and is sampled by the spectrum analyzer, which is termed the transmitted PIM. In this experiment, the third-order PIM signal at 710 MHz is measured.

The experimental results are shown in Figure 6. It indicates that as the microstrip line length increases, the forward PIM gradually rises while the reverse PIM exhibits oscillatory behavior, which is consistent with the experimental findings by other researchers [12].

Based on the formulas for forward and reverse PIM derived from the coated transmission-line model, Eq. (19), the experimental data are fitted. Here, the input currents I_1 and I_2 can be calculated from input power, leaving $\delta \mu_r^{(3)}$ as the only unknown parameter. By performing the fit, the value of $\delta \mu_r^{(3)}$ can be extracted. According to the fitting results shown in Figure 6, it is found that $\delta \mu_r^{(3)} = 0.48 \times 10^{-10}\ \mathrm{m^3/A^2}$.

For the LNS-FDTD full-wave method, since $\delta \mu_r^{(3)}$ is also the only unknown simulation parameter, an appropriate value of $\delta \mu_r^{(3)}$ is adjusted until the simulation results match the experimental measurements, thereby determining the parameter $\delta \mu_r^{(3)} = 1 \times 10^{-10}\ \mathrm{m^3/A^2}$. The corresponding simulation results are also shown in Figure 6. It can be seen that the nonlinear parameters obtained by the transmission-line method and the full-wave method are in good agreement, which verifies the feasibility of the proposed extraction method. Taking the ratio of the two to evaluate the deviation between the two methods, the deviation is given by $e = \frac{1\times10^{-10}}{0.48\times10^{-10}} = 6.4\mathrm{dB}$.

Limitation of the extraction methods

In the transmission-line method, an equivalent circuit model is employed to derive the analytical expressions for the PIM of the ferromagnetic-material-coated microstrip line. A key assumption that could introduce error is the coupling efficiency $\xi \approx k_0$. This

https://doi.org/10.1017/S1759078726103572 Published online by Cambridge University Press

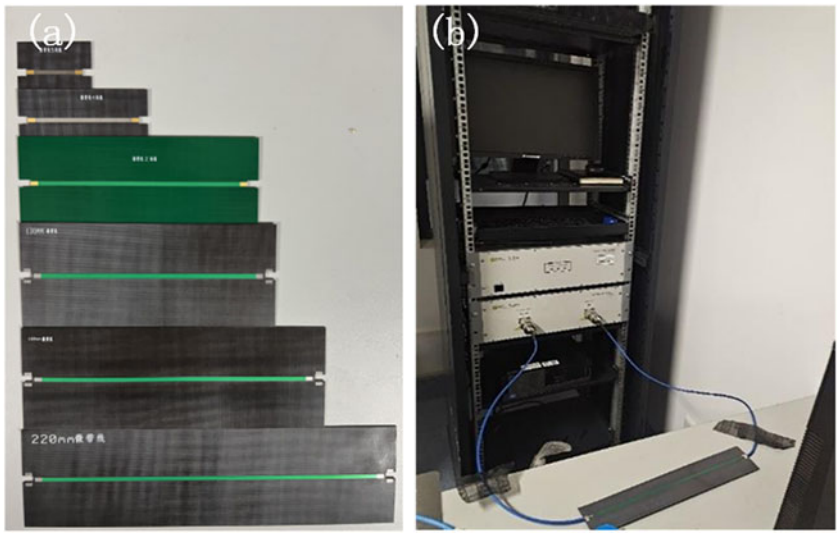


Figure 4. Photos of (a) the nickel-plated microstrip lines and (b) the PIM test equipment.

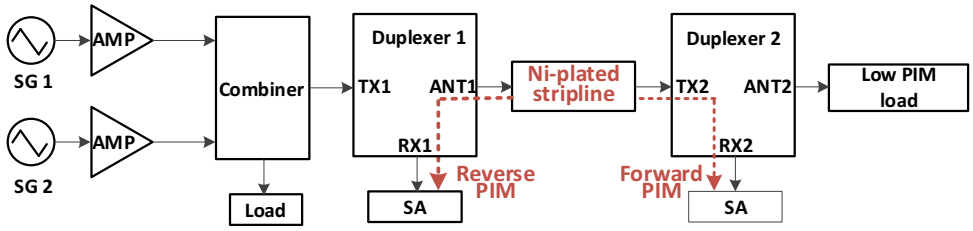


Figure 5. Schematic diagram of the PIM test system.

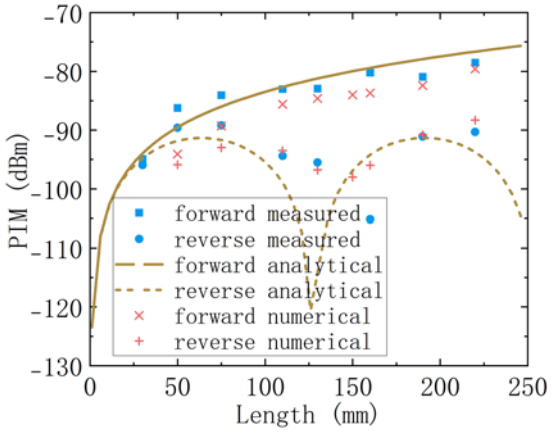


Figure 6. PIM results as the function of the length of the microstrip line obtained from the experiments, the coated-microstrip-line-model analytical equations, and the LNS-FDTD full-wave numerical calculation. The experimental data are obtained from Ref. [17].

coupling coefficient represents the efficiency with which the nonlinear field generated in the ferromagnetic-material coating couples back into the microstrip line and is subsequently absorbed by the load. In reality, however, because the nonlinear field is primarily generated above the microstrip line, a significant portion is lost due to radiation. Only a fraction of couples back into the line, resulting in an actual coupling efficiency $\xi < k_0$. Therefore, this can lead to an underestimation of the extracted nonlinear coefficient.

Furthermore, the proportionality coefficient k_0 also needs further discussion. As shown in the magnetic field distribution in Figure 7(a), the current density on the upper and lower surfaces of the upper conductor is not uniform across the conductor width. In the fitting performed in the "PIM experiments" section, the ratio of current densities at the center of the conductor was taken as the value of k_0, which is obtained to be 0.17. We note that this approach for determining k_0 also requires further investigation to improve the accuracy of nonlinear parameter extraction.

With respect to the full-wave method, it is necessary to obtain the magnetic field values at the conductor surface. However, since the conductor boundary lies on the Yee grid boundary, the tangential magnetic field on the conductor surface is not directly defined in the FDTD calculation, requiring interpolation. In this work, we use the magnetic field value at the nearest grid point as an approximation, which we identify as the primary source of error in extracting nonlinear parameters via the full-wave method. Evidently, reducing the mesh size brings the nearest-grid magnetic field closer to the actual surface field, thereby improving simulation accuracy. Figure 7(b) presents the computed PIM values under different nearest-grid mesh sizes. It can be observed that as the mesh size decreases, the PIM tends to increase. Hence, it can be inferred that the nonlinear parameter extracted by the full-wave method will be larger than its actual value.

Due to the constraint of the Courant stability condition, reducing the mesh size requires a corresponding decrease in the time step, which significantly increases the simulation time and thus limits the extent to which the mesh can be refined. In the future, the Hybrid Implicit Explicit (HIE)-FDTD algorithm [18] could be considered, as it relaxes the time-step restriction while still allowing a finer mesh in the z-direction.

https://doi.org/10.1017/S1759078726103572 Published online by Cambridge University Press

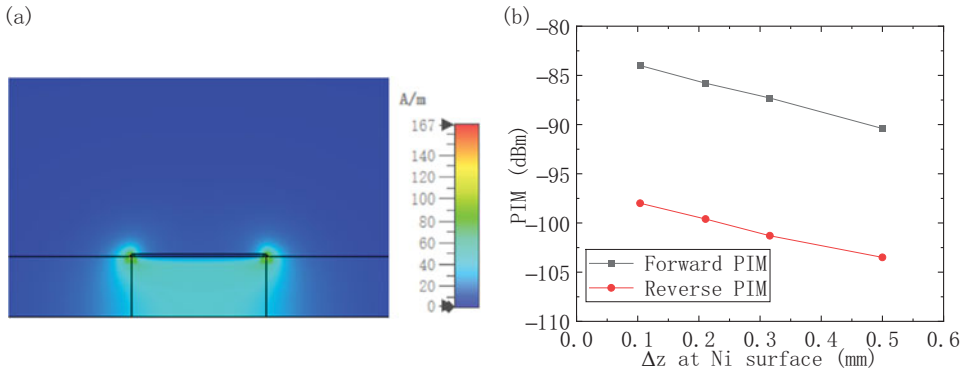


Figure 7. (a) The H_x field distribution of the coated microstrip line; and (b) the calculated PIM as a function of the mesh size Δz at the nearest grid of the nickel surface.

As described in the above section, the nonlinear parameter extracted by the LNS-FDTD full-wave method is larger than that obtained by the coated transmission-line model, which is consistent with the above analysis.

Conclusion

In this work, we propose intrinsic nonlinear parameter extraction methods for microwave ferromagnetic materials, which are critical to understanding PIM and radiated spurious emissions. The ferromagnetic material is coated or plated on the surface of a microstrip line, and its PIM effect is measured. We define the product of the skin depth and the nonlinear permeability as the intrinsic nonlinear parameter. Analytical equations for the relationship between the intrinsic nonlinear parameter and the PIM value are derived based on the transmission-line theory, and then the parameter is extracted from fitting the experimental results, which is called the coated transmission-line method. Additionally, we proposed an LNS-FDTD full-wave method. The LNS-FDTD simulation method is based on the nonlinear nature of the ferromagnetic material, in which the intrinsic nonlinear parameter is also the only unknown parameter. Therefore, we can extract the parameter by comparing the simulation results with the experimental data. A nickel-plated microstripline is used to verify these two methods. The extracted results are in good agreement. To further improve extraction accuracy, future work should focus on refining the coupling efficiency approximation in the coated transmission-line method and improving the magnetic field approximation at the conductor surface in the LNS-FDTD full-wave method.

Competing interests. The authors report no conflict of interest.

References

1. **Ge J, Wang T, Peng Y and Wang G** (2022) Electrically tunable microwave technologies with ferromagnetic thin film: Recent advances in design techniques and applications. *IEEE Microwave Magazine* **23**(11), 48–63. https://doi.org/10.1109/MMM.2022.3196415
2. **Testov OA, Komlev AE, Gareev KG, Khmelnitskiy IK, Luchinin VV, Sevost'yanov EN and Testov IO** (2021) Providing a specified level of electromagnetic shielding with nickel thin films formed by DC magnetron sputtering. *Coatings* **11**(12), 1455. https://doi.org/10.3390/coatings11121455
3. **Celozzi S, Araneo R, Burghignoli P and Lovat G** (2022) *Electromagnetic Shielding: Theory and Applications*. Newark: John Wiley & Sons.
4. **Kikitsu A, Kurosaki Y, Iwasaki H, Fujita A, Nishigaki H and Matsunaka S** (2021) Wide band direct on-chip EMI shielding layer with metallic/magnetic multilayer. *Journal of Magnetism and Magnetic Materials* **539**, 168339. https://doi.org/10.1016/j.jmmm.2021.168339
5. **Bas DA, Shah PJ, Matyushov A, Popov M, Schell V, Budhani RC, Srinivasan G, Quandt E, Sun N, and Page MR** (2021) Acoustically driven ferromagnetic resonance in diverse ferromagnetic thin films. *IEEE Transactions on Magnetics* **57**(2), 1–5. https://doi.org/10.1109/TMAG.2020.3019214
6. **Shlepnev Y and McMorrow S** (2011) Nickel characterization for interconnect analysis In *2011 IEEE International Symposium on Electromagnetic Compatibility*. Long Beach, CA, USA,: IEEE, pp. 524–529.
7. **De Sabata A and Ignea A** (2013) Passive intermodulation distortions induced by ferromagnetic materials at GSM frequencies. In *International Symposium on Signals, Circuits and Systems ISSCS2013*. Iasi, Romania, pp. 1–4.
8. **Henrie J, Christianson A and Chappell WJ** (2008) Prediction of passive intermodulation from coaxial connectors in microwave networks. *IEEE Transactions on Microwave Theory and Techniques* **56**(1), 209–216. https://doi.org/10.1109/TMTT.2007.912166
9. **Jin Q, Gao JC, Flowers GT, Wu YL, Xie G, and Bi LY** (2019) Modeling of passive intermodulation in connectors with coating material and iron content in base brass. *IEEE Transactions on Microwave Theory and Techniques* **67**(4), 1346–1356. https://doi.org/10.1109/TMTT.2019.2893193
10. **Jin Q and Feng Q** (2021) Passive intermodulation distortion in connectors with nonlinear interaction in electrical contacts and magnetic materials. *IEEE Transactions on Microwave Theory and Techniques* **70**(2), 1119–1131. https://doi.org/10.1109/TMTT.2021.3123334
11. **Zhang K, Li K and Cui W** (2025) Design and implementation of a passive intermodulation test platform for micro samples In *2025 IEEE MTT-S International Wireless Symposium (IWS)*. Xi'an, China: IEEE, 1–3.
12. **Kozlov DS, Shitvov AP and Schuchinsky AG** (2015) Passive intermodulation in distributed circuits with cascaded discrete nonlinearities In *2015 9th European Conference on Antennas and Propagation (Eucap)*. Lisbon, Portugal, pp. 1–5.
13. **Zhao X, He Y and Zhang A** (2023) Linearity–nonlinearity-separation FDTD method for nonlinearity analysis of passive microstrip circuits. *IEEE Microwave and Wireless Technology Letters* **33**(10), 1407–1410. https://doi.org/10.1109/LMWT.2023.3309666
14. **Zhao X, He Y and Zhang A** (2024) Closed-form equation for passive intermodulation of microstrip line due to resistivity nonlinearity. In *2024 IEEE 7th International Conference on Electronic Information and Communication Technology (ICEICT)*. Xi'an, China, pp. 851–853.
15. **Zhao X, He Y and Zhang A** (2024) An intermodulation matrix method for PIM evaluation of microstrip circuit. In *2024 IEEE 7th International Conference on Electronic Information and Communication Technology (ICEICT)*. Xi'an, China, pp. 842–844.
16. **Zhao X, He Y and Zhang A** (2024) Full-wave simulation of contact-nonlinearity-induced passive intermodulation using a nonlinear interface

boundary model. *IEEE Microwave and Wireless Technology Letters* **34**(6), 583–586. https://doi.org/10.1109/LMWT.2024.3381953

17. **Zhou HN, Zhao XL, Peng YB, Zeng MQ, Cao Z, Zhang KY, and He YN** (2023) Transfer matrix theory for passive intermodulation of microstrip lines. *Journal of Terahertz Science and Electronic Information Technology* **21**(7), 856–863.
18. **Chen J**. (2018) A review of hybrid implicit explicit finite difference time domain method. *Journal of Computational Physics* **363**, 256–267. https://doi.org/10.1016/j.jcp.2018.02.053



Xiaolong Zhao received his B.E. degree in microelectronics and Ph.D. degree in electronics science and technology, Xi'an Jiaotong University in 2012 and 2017, respectively. He worked as an engineer engaged in signal distortion solution for the smartphone at Huawei Technology Co., Ltd. He is currently an associate professor in the School of Microelectronics at Xi'an Jiaotong University. His research interests include nonlinear interference modeling and electromagnetic simulation for RF components, and semiconductor-devices and systems for nuclear radiation detection.



Xiaojian Xiang received the B.Sc. and M.Sc. degrees in mechanical engineering and automation from Northeastern University, China, in 2012 and 2014, respectively, and the Ph.D. degree in electronic science and technology from Shanghai Jiao Tong University, China, in 2019. He was a Joint Post-Doctoral Fellow at Tsinghua University and the Research Institute of Tsinghua University in Shenzhen. He is currently an Associate Director and Researcher at the Research Institute of Tsinghua University in Shenzhen, serving as the Deputy Director of the Superlubricity Technology Research Institute. His research interests include electrostatic RF-switches, electrostatic actuators, inertia switches, and superlubricity-based MEMS/NEMS devices.

https://doi.org/10.1017/S1759078726103572 Published online by Cambridge University Press